https://dx.doi.org/10.1016/j.enconman.2022.115560

Multi-objective optimizations of solid oxide co-electrolysis with intermittent renewable power supply via multi-physics simulation and deep learning strategy

Yi Sun[1], Jiong Lu[1], Qiuhua Liu[1], Wei Shuai[2, **], Anwei Sun[2], Nan Zheng[2], Yu Han[2], Gang Xiao[2, **], Jin Xuan[3], Meng Ni[4], Haoran Xu[2, *, **]

[1] Power China Huadong Engineering Co. Ltd., Hangzhou 310014, PR China

[2] State Key Laboratory of Clean Energy Utilization, Zhejiang University, 38 Zheda Road, Hangzhou, 310027, China

[3] Department of Chemical Engineering, Loughborough University, Loughborough, United Kingdom

[4] Department of Building and Real Estate, Research Institute for Sustainable Urban Development (RISUD) & Research Institute for Smart Energy (RISE), Hong Kong Polytechnic University, Hung Hom, Kowloon, Hong Kong, China

Abstract: Solid oxide electrolysis cell (SOEC) is a novel approach to utilize excess renewable power to produce fuels and chemicals. However, the intermittence and fluctuation of renewable energy requires more advanced optimization strategy to make sure its performance in safety and cost-effectiveness. Here, we propose a hybrid model for the precise and quick optimization of the co-electrolysis process in the SOEC for syngas production, based on the multi-physics simulation (MPS) and deep learning algorithm. The hybrid model fully considers electrochemical/chemical reactions, mass/momentum transport and heat transfer, and presents a small relative error (< 1%) in most the cases (> 96%). Various targets including the single-objective, dual-objective

and multi-objective optimizations are evaluated with particular attentions on the reactant conversion rate and energy efficiency at different temperatures. The electrolysis efficiency is negatively correlated with the power supply in all strategies and thermal neutral condition (TNC) can be achieved at different temperatures, where 1023 K, 1053 K, 1083 K and 1113 K are corresponded to the TNC power range of 10-16 W, 14-23 W, 18-29 W and 22-37 W, respectively. This theory can be flexibly applied in the sustainable manufacturing and circular economy sectors and energy according to the optimization targets.

Keywords: Solid oxidation electrolysis cell; Renewable powers; Numerical simulation; Deep learning; Co-electrolysis.

* Corresponding authors Email: haoranxu@zju.edu.cn (Haoran Xu)

** The three authors have the same contribution to this study

1. Introduction

Our reliance on fossil fuels has led to a lot of global challenges such as climate change, environment pollution and energy crisis [1]. A systemic transition to clean energy is urgently needed to realize the net-zero economy and carbon-neutral society [2, 3]. Hydrogen-based energies are potential choices to replace fossil fuels as they are environmentally friendly and high-energy-density in mass [4, 5]. On the other hand, many scholars are working on electrochemical CO_2 reduction into fuels or chemicals for cleaner provision of energy and achieving circular economies [6-8]. Therefore, co-electrolysis of H_2O and CO_2 with renewable powers is crucial to achieve zero emission and meet global sustainable energy needs as it not only provides an alternative method for energy generation but also efficiently captures and reduces CO_2 [9].

SOEC is a promising technology because of its high efficiency, fast kinetics and wide reactant selections [10, 11]. Compared with low temperature electrolysis technologies, the high operating temperature brings thermodynamic advantages and less overpotential losses especially in the co-electrolysis of H_2O and CO_2 [12, 13]. However, the high temperature operation also causes extra difficulties in thermal management and performance optimization in achieving a high-power density and energy efficiency [14]. With the change of operating parameters, SOECs can work in endothermic or exothermic status, which plays as a key indicator for its performance evaluation [15]. Optimization strategies are thus necessary to adjust the operating conditions and meet the desired criteria especially when directly driven by intermittent renewable powers [16-19].

System-level simulation has proven that the combination of SOEC and renewable power like solar and wind energy can make full use of energy and get high cost-effectiveness [20, 21]. But the exact operating conditions of SOEC when utilizing fluctuating renewable energies were not considered, which not only caused uncertainty in the production rate but also made it difficult to keep a safe operating environment with high energy efficiency. To solve this problem, dynamics models of SOEC were developed to investigate the effects of input power fluctuation on the SOEC temperature and efficiency [22-24]. To reduce the computing resources and make it applicable for the real-time optimization, Han et al. [25] also proposed a black-box model to represent the dynamic models to reduce cost and computing-time. Qiong et al. [26] further studied the single-target optimization such as the hydrogen production, energy consumption and compressor consumption for the SOEC. But these studies missed the real-time operating parameters with actual fluctuating power supply and lacked the competence for the multi-objective optimizations of SOECs. A new method is thus needed for the fast and accurate multi-objective optimization of SOECs with cost-effectiveness and high efficiency.

Considering the highly coupled physical/chemical processes and complex operating conditions in the SOEC [27], multi-physics simulations (MPS) are widely adopted to investigate the performance at various parameters [28-31]. To meet the high calculation demands of MPS for the purpose of real-time optimization, its combination with artificial intelligence (AI) has been proposed [32-35]. Among the AI algorithms, machine learning (ML), fuzzy logic and heuristic optimization are the most commonly

used [36], where deep neural networks (DNN) is regarded as an efficient tool in the field of non-linear systems [37, 38]. Due to the black-box nature, DNN is particularly suitable for the engineering applications [39, 40], and fast optimization can be achieved with the further combination with optimization algorithms such as genetic algorithm (GA) [41].

Along this line, here we perform a case study on photovoltaic-SOEC integrated system to demonstrate the effectiveness of the proposed concept. Photovoltaic is chosen because of its economic benefits in power generation, but its intermittent power generation nature requires solutions in the direct utilization in the electrolysis process [42, 43]. In this study, to solve the challenges, a hybrid model by combining experimental data, MPS, DNN and GA is developed to quickly and accurately obtain the best working conditions corresponding to the fluctuating power supply under different optimization objectives.

2. Model development

As shown in Fig. 1, we choose output power data in a typical day from a photovoltaic power station as the input profile of power supply. We assume the total PV power is evenly dispersed into the SOEC units by a transformer. With a certain input power from PV, the applied voltage in SOEC can be set as the values needed. The proposed scheme includes the development of MPS model with the validation of experimental data, the extension of database with the scanning sets of input/output parameters for the training of DNN model, and the GA prediction of optimized parameters of SOEC at different strategies.

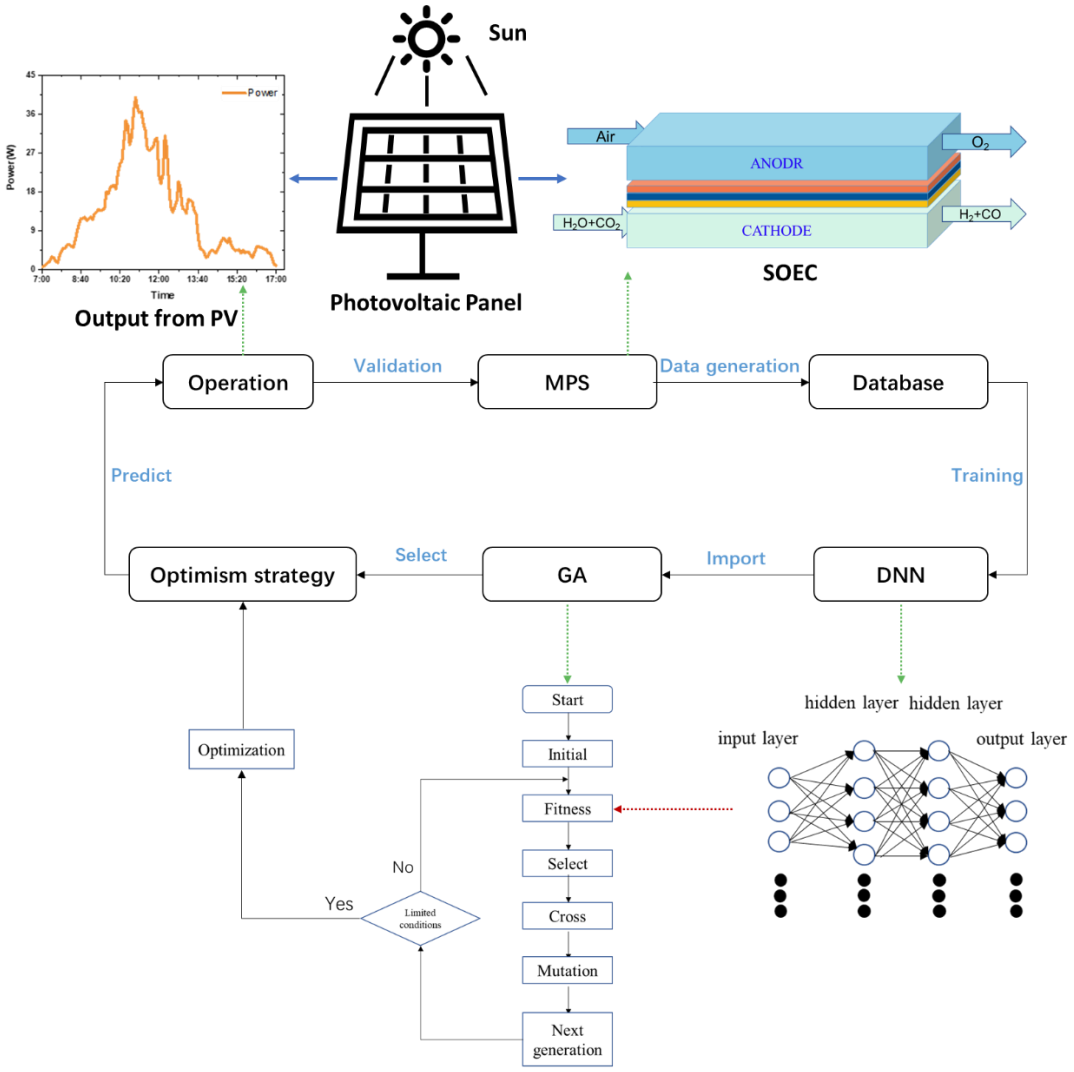

Fig. 1. Schematic of the hybrid model.

2.1 Development of MPS model

Based on the experimental data [44], the thicknesses of cathode support layer (Ni-YSZ), cathode active layer (Ni-ScSZ), electrolyte (ScSZ) and anode (LSM-ScSZ) in the tubular SOEC are 760 μ m, 10 μ m, 10 μ m and 15 μ m, respectively. Key properties of the SOEC material and reaction parameters used in the model are listed in Table 1 & 2.

Table 1. Properties of the adopted materials

Parameters	Value or expression	Unit
Conductivity		

σ_{ScSZ}	$69{,}200 \times e^{\frac{-9681}{T}}$	S m^{-1}
σ_{YSZ}	$33{,}400 \times e^{\frac{-10300}{T}}$	S m^{-1}
σ_{Ni}	4.2×10^{6}-1,065.3T	S m^{-1}
σ_{LSM}	4.2×10^{7}exp(-1,150/T)	S m^{-1}
Porosity		
ε_a	0.36	
ε_c	0.36	
Tortuosity		
τ_a	3	
τ_c	3	
Triple Phase Boundary		
S_{TPB}	2.14×10^{5}	m^{-1}
Heat Conductivity		
λ_a	9.6	W m^{-1} K^{-1}
λ_c	6.23	W m^{-1} K^{-1}
λ_{el}	2.7	W m^{-1} K^{-1}
Heat Capacity		
$C_{p,a}$	420	J kg^{-1} K^{-1}
$C_{p,c}$	390	J kg^{-1} K^{-1}
$C_{p,el}$	300	J kg^{-1} K^{-1}
Density		
ρ_a	6,570	Kg m^{-3}
ρ_c	6,870	Kg m^{-3}
ρ_{cl}	2,000	Kg m^{-3}

Table 2. Kinetics of reactions.

Electrochemical Reaction		
i_o	$\beta \cdot \exp(-\frac{E_a}{RT})$	Am^{-2}
β	3.3×10^{8}	Am^{-2}
E_a	1.2×10^{5}	J mol^{-1}
∂_{H_2O}	0.6	
∂_{CO_2}	0.6	
Chemical Reaction		
R_{WGSR}	$K_{sf}\left(P_{H_2O}P_{CO} - \frac{P_{H_2}P_{CO_2}}{K_{ps}}\right)$	mol m^{-3}s^{-1}
K_{sf}	$0.0171\exp\left(\frac{-103191}{RT}\right)$	Pa $^{-2}$s^{-1}
K_{ps}	$exp\left(\begin{matrix}-0.2935Z^3 + 0.6351Z^2 \\ +4.1788Z + 0.31\end{matrix}\right)$	
Z	$\frac{1000}{T} - 1$	

In this section, we present a concise introduction of the governing equations. For model simplification, below assumptions and boundary conditions are adopted in the MPS model while more detailed conditions of the MPS model development can be found in our previous work [45, 46] .

Assumption：

(1) Gases in SOEC are all ideal gases.

(2) Electrochemical reactions only take place at triple-phase boundaries.

(3) Heat loss including thermal radiation and thermal convection between the SOEC and environment is neglected.

(4) H_2/H_2O and CO/CO_2 are the main reactants in electrochemical reactions.

Boundary condition：

(1) At the chamber inlets of anode and cathode, the values of inlet gas flow rate, inlet gas composition, inlet gas temperature are set.

(2) At the outlets of chamber at anode and cathode, free flow condition is set.

(3) At the outside surfaces of the anode and cathode, the values of applied voltage are set.

(4) At the ends of electrodes and outside surface of the SOEC, zero flux and thermal insulation are set.

2.1.1. Electrochemical reactions

The mixture of H_2O and CO_2 flows through the cathode channel, and they are reduced as shown in Eqs. (1)-(2).

$$H_2O + 2e^- = H_2 + O^{2-} \quad (1)$$

$$CO_2 + 2e^- = C0 + 0^{2-} \quad (2)$$

O^{2-} ions then are transported to the anode, where electrons are released and O_2 is generated as shown in Eq. (3).

$$O^{2-} = 0.5O_2 + 2e^- \quad (3)$$

The applied voltage can be calculated by Eq. (4).

$$V = E_{eq} + \eta_{act} + \eta_{ohmic} \quad (4)$$

Where, calculations of the E_{eq} for H_2O and CO_2 are given in Eqs. (5) and (6), respectively, and calculations of the η_{act} is shown in Eq. (7), and η_{ohmic} is calculated by Ohm's law as given in Eqs. (8) and (9).

$$E_{eq,H_2O} = E^0_{eq,H_2O} + \frac{RT}{2F} ln \left[\frac{P^{L,C}_{H_2} (P^{L,A}_{O_2})^{1/2}}{P^{L,C}_{H_2O}} \right] \quad (5)$$

$$E_{eq,CO_2} = E^0_{eq,CO_2} + \frac{RT}{2F} ln \left[\frac{P^{L,C}_{CO} (P^{L,A}_{O_2})^{1/2}}{P^{L,C}_{CO_2}} \right] \quad (6)$$

$$i = i_0 \left\{ exp\left(\frac{\alpha n F \eta_{act}}{RT}\right) - exp\left(-\frac{(1-\alpha) n F \eta_{act}}{RT}\right) \right\} \quad (7)$$

$$i_1 = -\sigma_1^{eff} \nabla(\emptyset_1) \quad (8)$$

$$i_s = -\sigma_s^{eff} \nabla(\emptyset_s) \quad (9)$$

2.1.2 Chemical reactions

The reversible water-gas shift reaction (WGSR) is also considered as shown in Eq. (10)

$$CO + H_2O \leftrightarrow CO_2 + H_2 \quad (10)$$

2.1.3 Mass/momentum transport

Considering the Knudsen diffusion and free molecule diffusion in channels and porous layers, the mass transport of the gas species is calculated as shown in Eq. (11).

$$\frac{N_i}{D_{ik}^{eff}} + \sum_{j=1.j\neq i}^{n} \frac{y_i N_j}{D_{ij}^{eff}} = -\frac{1}{RT}\left(\nabla(y_i P) + \frac{B_0 y_j P}{\mu D_{ik}^{eff}}\nabla P\right) \quad (11)$$

The mentum transport is calculated as shown in Eq. (12).

$$\rho\frac{\partial u}{\partial t} + \rho u\nabla u = -\nabla p + \nabla\mu\left[(\nabla u + (\nabla u)^T) - \frac{2}{3}\mu\nabla u\right] - \frac{\varepsilon\mu u}{k} \quad (12)$$

2.1.4 Heat transfer

The heat transfer process is calculated as shown in Eq. (13).

$$\rho C_P u \cdot \nabla T + \nabla \cdot \left(-\lambda_{eff}\nabla T\right) = 0 \quad (13)$$

2.2 Development of deep neural networks (DNN)

DNN is a typical artificial intelligence technology modeled after the biological neural networks, which can get a quick and accurate output through a given input without knowing the actual function between the input and output. Its network structure consists of an input layer, multiple hidden layers, and an output layer in which the connection between each layer is a series of weight matrix that is crucial for DNN. The outputs from the prior layer are propagated to the next layer as inputs by the activation function like ReLu.

In this particle, a six-hidden-layer back-propagation DNN is built with four inputs and four outputs while 256 neurons are used in each hidden layer. Linear is chosen as activation function in input layer and output layer while ReLU is chosen as activation function in hidden layers. The variables in input layer are the operating voltage, the current density, the inlets temperature and the cathode inlet gas composition. Meanwhile, the outputs in output layer are the cathode inlet gas flow rate, the cathode outlet gas composition (H_2 and CO) and the heat generation.

The training set, validation set and testing set account for 60%, 20%, 20%, respectively,

which constitute a 30090 x 8 data matrix. The epoch and batch size are set as 1000 and 50, respectively.

As the parameters have different orders of magnitude ranging from 10^{-2} to 10^{3}, the parameters are firstly normalized to the same range as shown in Eq. (14) to eliminate the influence of unit and scale differences between different features and get high accuracy of DNN.

$$x_i = 0.8\left(\frac{x-\min}{\max-\min}\right) + 0.2 \quad (14)$$

Here, x_i, x, max, and min are the value after normalization, the true value, the minimum value and the maximum value, respectively.

2.3 Genetic algorithm

GA is a method to search for optimal solution by simulating nature evolution. When solving complex combinatorial optimization problems, it can quickly obtain better optimization results compared with some conventional optimization algorithms. In this work, the population, generation, crossover and mutation rate of GA are set as 200, 200, 0.8 and 0.01 respectively. The optimization criterion varies from the different optimization strategies in section 3.2 – 3.4.

3.Results and discussion

3.1 Model validation

As shown in Table s1, the MPS model was validated by the comparison between the simulation results and experimental data at the same operating conditions. Good agreements were achieved at both 973 K (r = 0.994) and 1023 K (r = 0.992) as shown in Fig. 2(a). A database was then built based on the proposed MPS model to extend the

primary operating parameters (temperature, gas composition, operating voltage, flow rate) and the primary performance parameters (power consumption, heat generation, conversion rate, etc.). The operating parameters of database are listed in Table s1 and the MPS results are listed in Table 3.

For the DNN model, the predicted results showed a small relative error (< 1%) in almost all cases (> 96%) as shown in Fig. 2(b). In the training set, it shows a high correlation coefficient (0.99983) and low root-mean-square errors (RMSE) (0.00226). As well as in the testing set, the correlation coefficient and RMSE are 0.99978 and 0.00254, respectively.

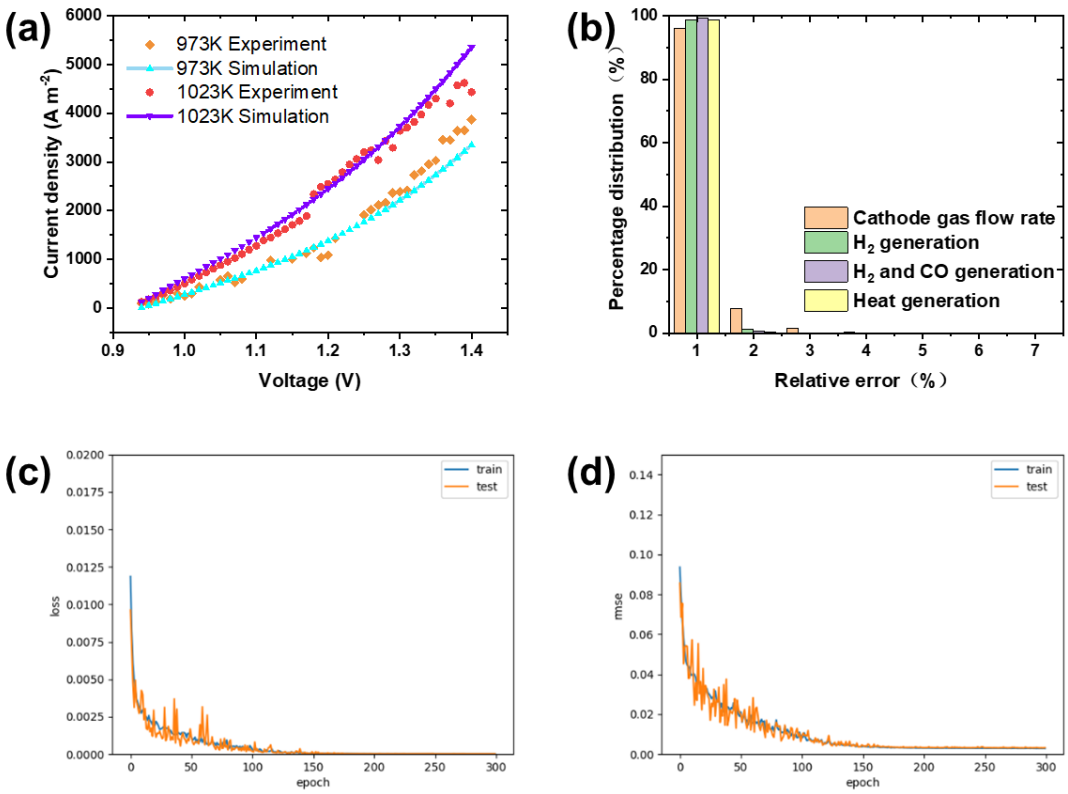

Fig. 2. (a). The simulation data and experiment data at different temperatures, (b). the values of relative errors in predicting the cathode gas flow rate, H_2 generation, H_2 and CO generation, heat generation using DNN, the change of loss (c) and RMSE (d) in training and testing sets with increasing epochs.

Table 3. The results of MPS model.

Parameter	Value	Unit
Current density	38.06 - 30309.6	A cm^{-2}
H_2 generation	0.02 - 87.52	%
total conversion rate	1 - 98.89	%
Heat generation	-1.46 - 6.97	W

3.2 Single objective optimization strategy

3.2.1 Minimum absolute heat generation

Thermal-neutral condition (TNC) is a state where the heat generated or absorbed by SOEC reaches to zero in which it can keep its high efficiency without extra operation. This condition is also associated with the small peak-temperature-gradient (PTG), which is key to keep SOEC from thermal damage in the long-term operation. To achieve the TNC at different conditions, the performance of SOEC with minimum absolute heat generation is studied.

The operating voltage kept a similar changing tendency with the fluctuation of power supply, which significantly affects the minimum heat generation at 1023 K as shown in Fig. 3(a). A small heat generation (< 0.5 W) was possible in the period before 10:20 and after 12:30, but it could increase to a very large value (2.5 W) at 11:00, which would impair the efficiency and cause thermal damage. A higher operating temperature (1113 K) could significantly reduce the minimum heat generation especially at high input power conditions as shown in Fig. 3(b). Through optimization, the minimum heat generation could be limited between -0.7 W and 0.3 W during the whole day operation. It should be noted that a negative heat generation means additional heat supply to the SOEC is required, which can increase the electrical efficiency but auxiliary equipment is needed.

The effects of different operating temperature can be further interpreted by Fig. 3(c) & (d). The operating voltage showed a dominant influence in this strategy while other operating parameters changed accordingly as shown in Table s2. With the increase of cathode inlet temperature, the kinetics of electrochemical reactions were significantly increased. As a result, smaller voltages were needed at the same power supply, and more heat was consumed in the endothermic electrochemical processes. A higher inlet gas temperature contributed to a larger power range for the TNC, where 1023 K, 1053 K, 1083 K and 1113 K were corresponded to the TNC power range of 10-16 W, 14-23 W, 18-29 W and 22-37 W, respectively.

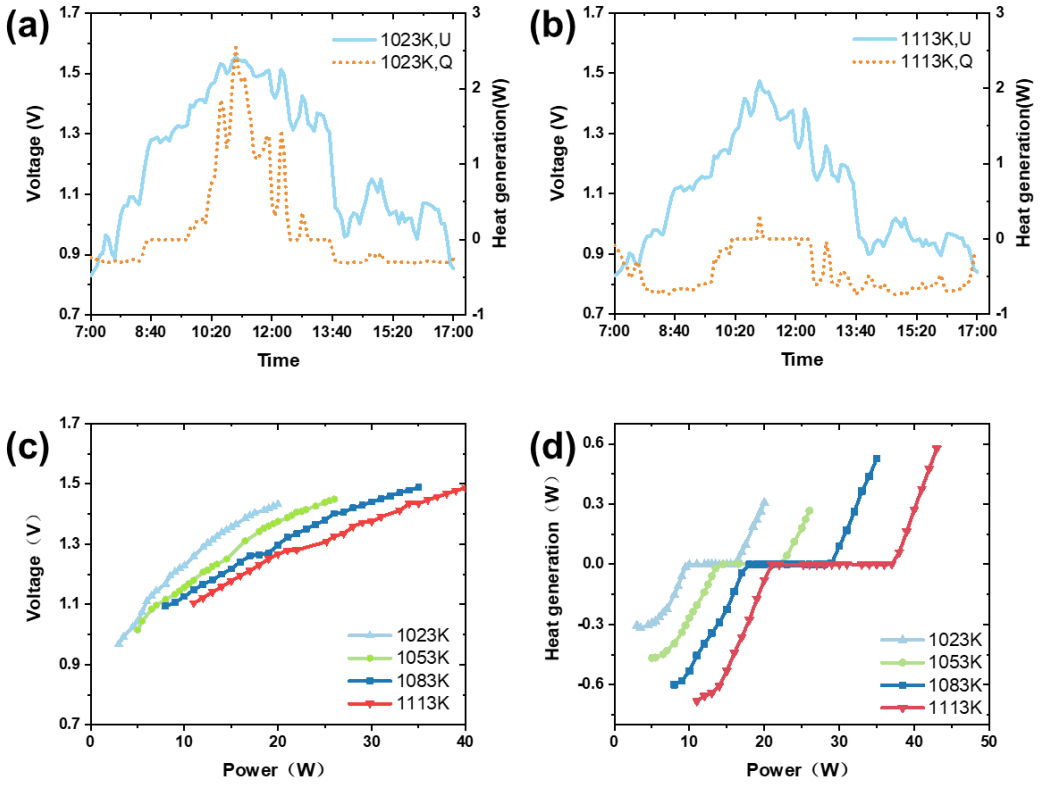

Fig. 3. The minimum absolute heat generation strategy. (a) the operating voltage and heat generation at 1023K - time relationship, (b) the operating voltage and heat generation at 1113K - time relationship, (c) the operating voltage changing with power at different temperatures, (d) the heat generation changing with power at different temperatures.

3.2.2 Maximum electrolysis efficiency

Electrolysis efficiency, as shown in Eq. (15), is vital to the economic operation of SOECs. A high efficiency (> 100%) not only fully utilizes the input electricity power, but also uses thermal energy as the drive force for the additional fuel generation. When combined with a concentrated solar thermal storage system, operating at such a high efficiency can bring more economic benefits.

$$\eta = \frac{\Delta H_H + \Delta H_C}{Q_{el} + Q_{th}} \tag{15}$$

Here, η is electrolysis efficiency, ΔH_H and ΔH_C are the high calorific value of hydrogen and carbon monoxide, respectively, Q_{el} and Q_{th} are the total electrical energy and total heat energy applied in system.

It can be observed in Fig. 4(a) & (b), the electrolysis efficiency decreased with growth of applied voltage. At 1023 K, the highest maximum efficiency (122%) was achieved at 7:00 and 17:00 while the lowest maximum efficiency (94%) was found at 11:00, indicating the importance of external heat energy supply at the beginning and ending phase. With the increasing operating temperature to 1113 K, the lowest maximum electrolysis efficiency was further increased to 99%, indicating that the additional thermal energy supply is needed during almost the whole period. The increase of gas temperature at inlets presented a stronger effect at smaller power supplies as can be seen from Fig. 4(c) & (d). Similarly, the operating voltage is the most important indicator. The voltage decreased by 0.09V and 0.1V, respectively, with the increasing temperature from 1023 K to 1113 K. In the meanwhile, the efficiency increased by 6.2% and 3.8% at 10 W and 40 W cases, respectively. Due to the negative

correlation of electrolysis efficiency and heat generation, a low H_2O composition (10%) and a high flow rate (> 500 SCCM) were favored while achieving the maximum electrolysis efficiency as shown in Table s3.

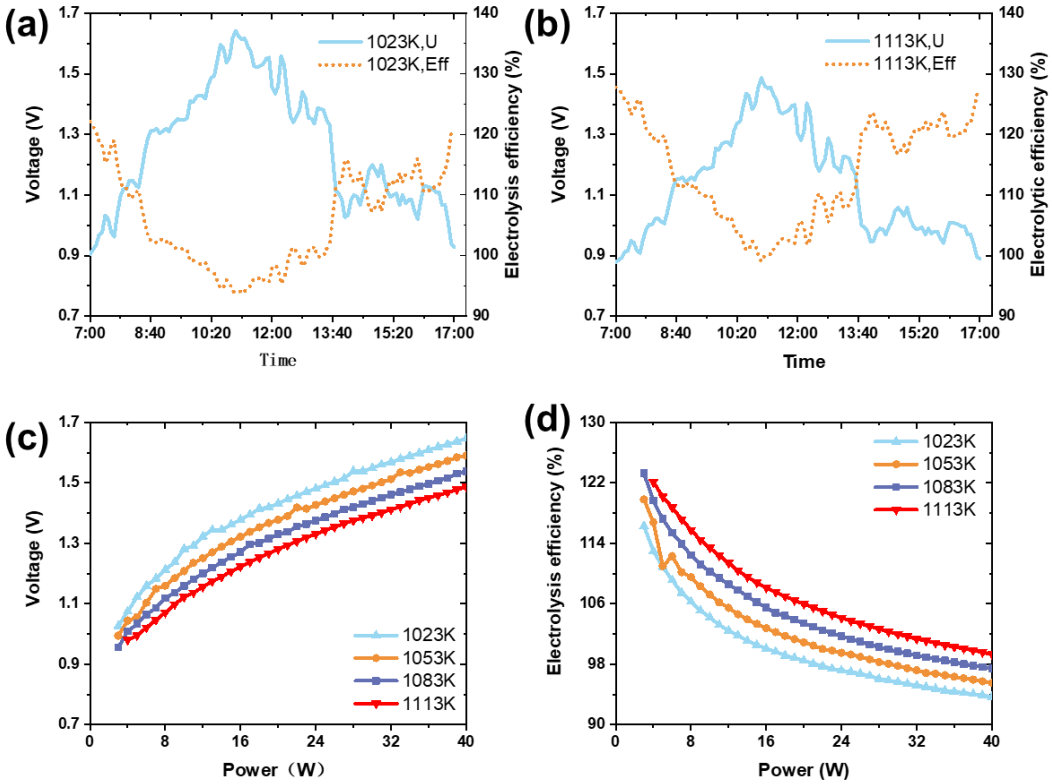

Fig. 4. The maximum electrolysis efficiency strategy. (a) the operating voltage and electrolysis efficiency at 1023 K - time relationship, (b) the operating voltage and electrolysis efficiency at 1113 K - time relationship, (c) the operating voltage changing with power at different temperatures, (d) the electrolytic efficiency changing with power at different temperatures.

3.2.3 Maximum conversion rate

Conversion rate is an essential indicator for the performance of SOECs. A high conversion rate means more H_2 and CO will be generated with the same condition at cathode inlet, which can bring more economic benefits. The conversion rate is expected to be as high as possible to get more products in industrial manufacture.

The operating voltage kept a similar changing tendency with the fluctuating power

supply, which significantly affected the maximum conversion rate at 1023 K as shown in Fig. 5(a). The smaller applied voltage was needed at high temperature (1113K) while the highest conversion rate, nearly 100%, was found at 11:00 as shown in Fig. 5(b). The maximum conversion rate remained over 60% from 10:20 to 11:55 at both temperatures.

Further research on the effects of temperature can be seen from Fig. 5(c) & (d). The maximum conversion rate is strongly affected by supply power while it shows little difference at different temperature. When the supply power reached to 40W, the maximum conversion rates at all temperatures nearly achieved 100% which means all the reactants are electrolyzed. Especially, the operating voltage showed an obvious transition at 33W because of the change of gas flow rate at cathode inlet. Moreover, the operating conditions of gas composition of H_2O remained 90% while the gas flow rate remained the lowest (300 SCCM) at small power supplies and grew slowly with the increase of power supplies when power supply was higher than 33W, as shown in Table s4.

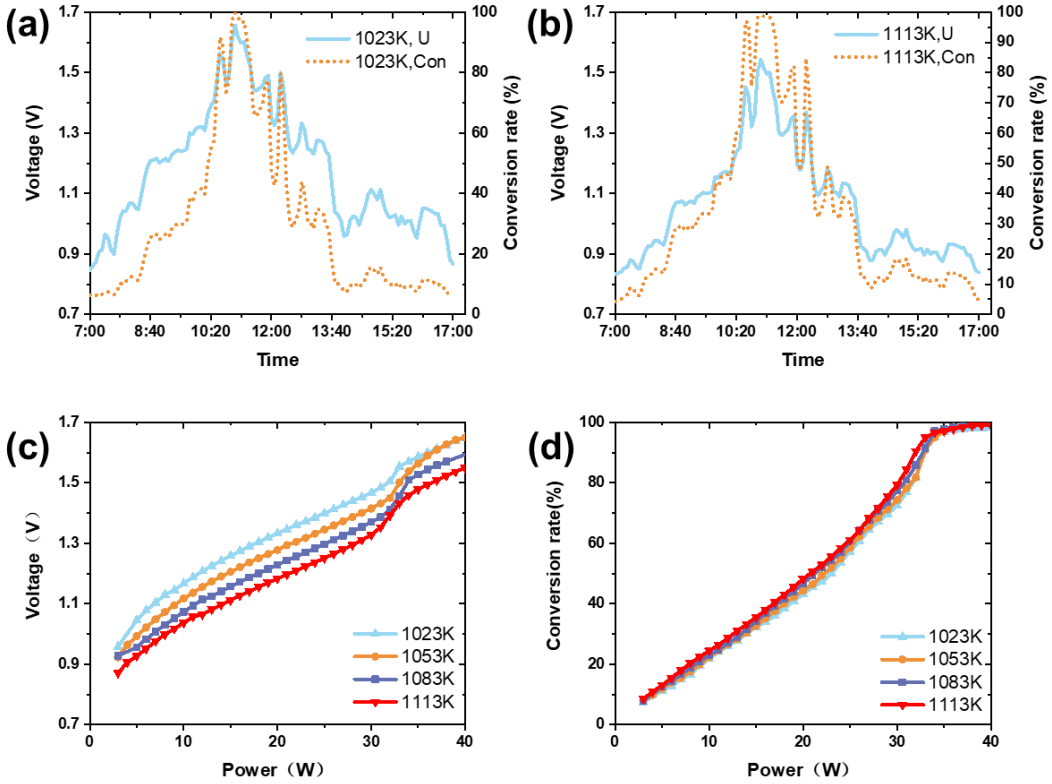

Fig. 5. The maximum conversion rate strategy. (a) the operating voltage and conversion rate of H_2 and CO at 1023 K - time relationship, (b) the operating voltage and conversion rate at 1113 K - time relationship, (c) the operating voltage changing with power at different temperatures, (d) the conversion rate changing with power at different temperatures.

3.3 Dual-objective optimization strategy

The indicators to evaluate the performance of SOEC are not limited to single object. The operation condition of maximum electrolysis efficiency contributes to a low conversion rate and low ratio of H_2:CO, which will affect the performance of SOECs. However, to bring more economic benefits, not only high electrolysis efficiency but also high conversion rate and high ratio of H_2 and CO are needed.

3.3.1 Maximum electrolysis efficiency while keeping the ratio of H_2:CO > 2:1

Since the caloricity of H_2 is higher than CO, a high ratio of H_2:CO is expected

while keeping maximum electrolysis efficiency. Because of the limiting condition of the generation ratio of H_2: CO, more H_2O was needed in cathode gas composition, causing a lower applied voltage and electrolytic efficiency at a certain output power compared with the strategy in Section 3.2.2 (Fig. 4(c) & Fig. 6(c)). It can be observed in Fig.6 (a)&(b), the highest operating voltage and the lowest electrolytic efficiency were 1.47 V, 91% (1023 K) and 1.3 V, 97% (1113 K), respectively, in the case of the highest power supply at 11:00. On the other hand, the increase of inlet gas temperature and power supplies presented a stronger effect at the maximum electrolytic efficiency (Fig. 6(d)). The operating voltage grew with the increase of supply power while the inlet gas composition of H_2O remained 90% to keep the ration of H_2:CO > 2:1 as shown in Table s5.

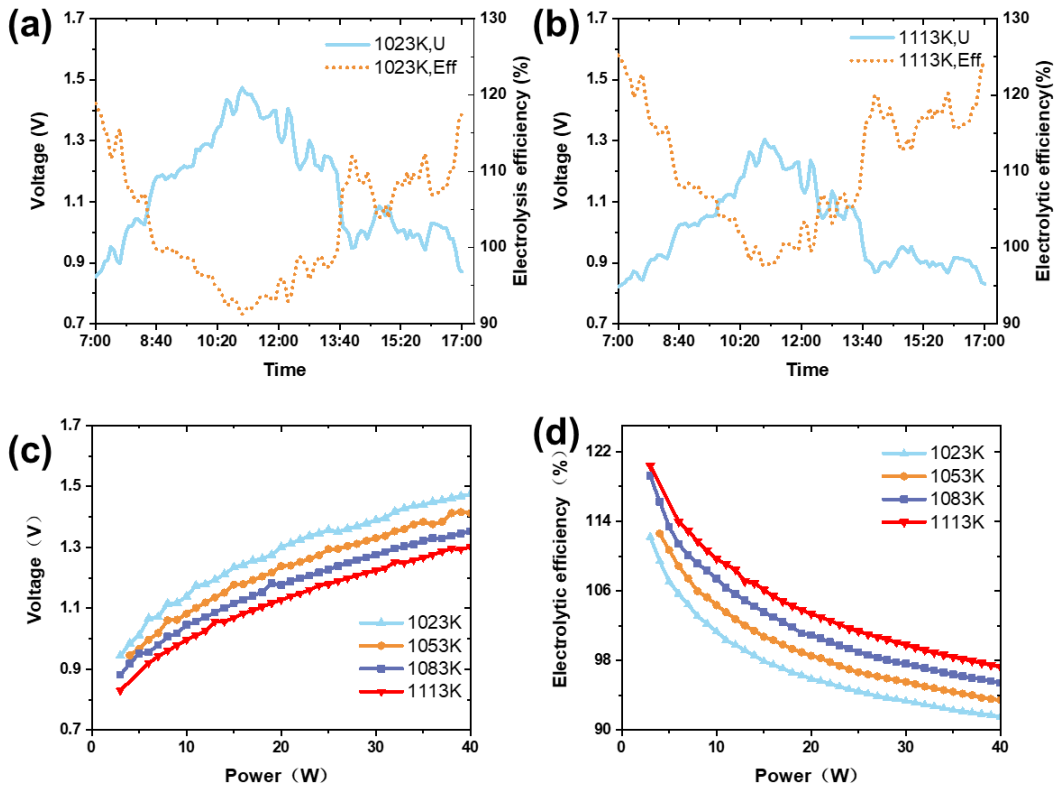

Fig. 6. Maximum electrolysis efficiency while keeping the ratio of H_2:CO > 2:1. (a) the operating voltage and electrolysis efficiency at 1023 K - time relationship, (b) the

operating voltage and electrolysis efficiency at 1113 K - time relationship, (c) the operating voltage changing with power at different temperatures, (d) the electrolytic efficiency changing with power at different temperatures.

3.3.2 Maximum conversion rate while keeping electrolysis efficiency>90%

Similarly, the operating conditions of the strategy of maximum conversion rate as shown in Fig. 5, contribute to a low electrolysis efficiency especially at high supply power. It follows that high heat generation affects the performance of SOECs.

Since the limited of the electrolysis, the conversion rate at low temperature (1023K) cannot achieve 100% even with the highest supply power, while the conversion rate at high temperature (1113K) got to 100% at 11:00 with the electrolysis efficiency of 91.6% as shown in Fig.7 (a)&(b). Compared with the strategy of maximum conversion rate at section 3.2.3, the restriction of electrolysis efficiency showed a great effect on the operating voltage and maximum conversion rate when the supply power was higher than 33W at low temperature (1023K & 1053K), conversely, the performance at high temperature (1083K & 1113K) was almost identical with the latter (Fig. 7(c) & (d)). Similarly, the operating inlet gas composition of H_2O kept 90% and the operating inlet gas flow remained 300 SCCM at first while it increased with the growth of the supply power after 33W as shown in Table s6.

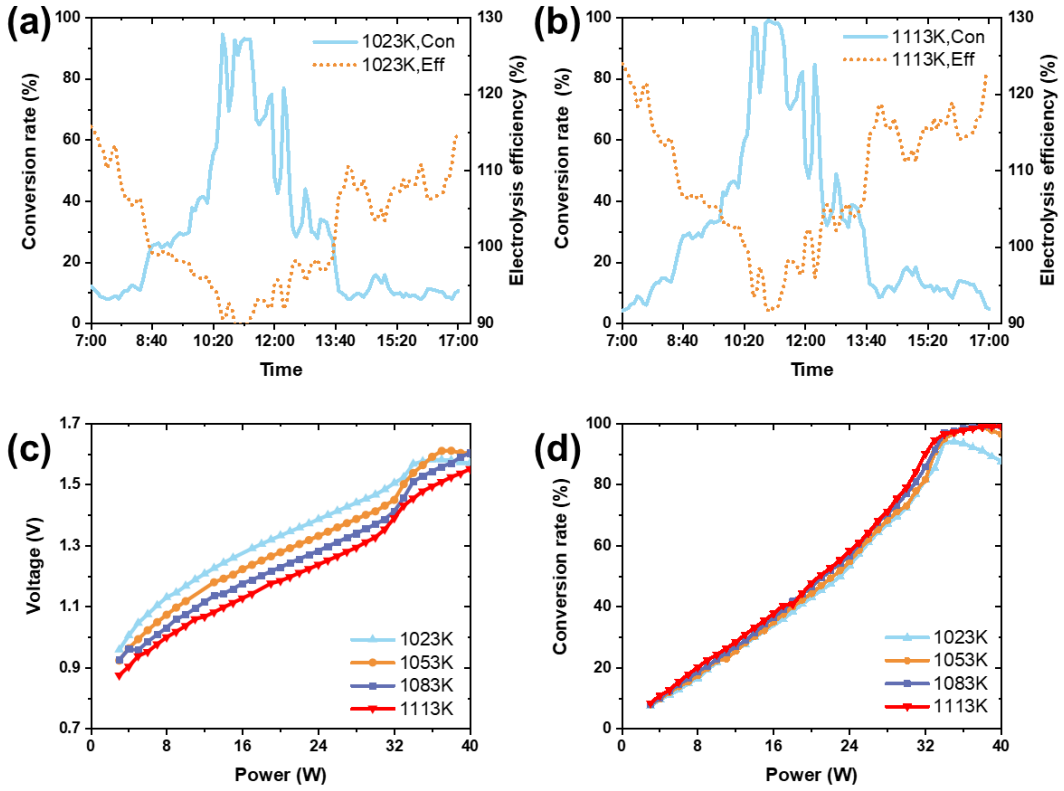

Fig. 7. Maximum conversion rate while keeping electrolysis efficiency>90%. (a) the conversion rate and electrolysis efficiency at 1023 K - time relationship, (b) the conversion rate and electrolysis efficiency at 1113 K - time relationship, (c) the operating voltage changing with power at different temperatures, (d) the conversion rate changing with power at different temperatures.

3.4 Multi-objective optimization strategy

A high production rate is usually desired especially in the industrial-level applications. In this section, we proposed different strategies to find the largest gas flow rate while keeping the ratio of H_2:CO > 2:1 and electrolysis efficiency>90%.

Interestingly, while keeping the ratio of H_2:CO > 2:1 and electrolysis efficiency>90%, the maximum gas flow rate can reach to 600 SCCM with any supply power, which means SOECs can work on the condition of 600 SCCM gas flow rate in the whole day. Moreover, the electrolysis efficiency at 1023K got to minimum (91.2%) with conversion rate of maximum (40.1%) and the electrolysis at 1113K got to

minimum (97.1%) with conversion rate of maximum (42.7%) at 11:00 as shown in Fig. 8(a) & (b). In general, the maximum conversion rates at both temperatures were more than 40% while we chose the largest gas flow rate, which can achieve high production.

Further research on the effect of temperature is shown in Fig. 8(c) & (d). The electrolysis efficiency showed a positive correlation to the temperature at high supply power, while the operating voltage decreased with the growth of temperature. When the supply power was 40W, the operating voltage got to 1.47V at 1023K with electrolysis efficiency of 91.2% while it only needed 1.31V at 1113K with electrolysis efficiency of 97.1%. Especially, when SOECs changed from endothermic state to exothermic state, the operating voltage showed a small drop while changing with the increase of supply power. The maximum operating fluid flow rate came to 600 SCCM with the inlet composition of H_2O as shown in Table s7.

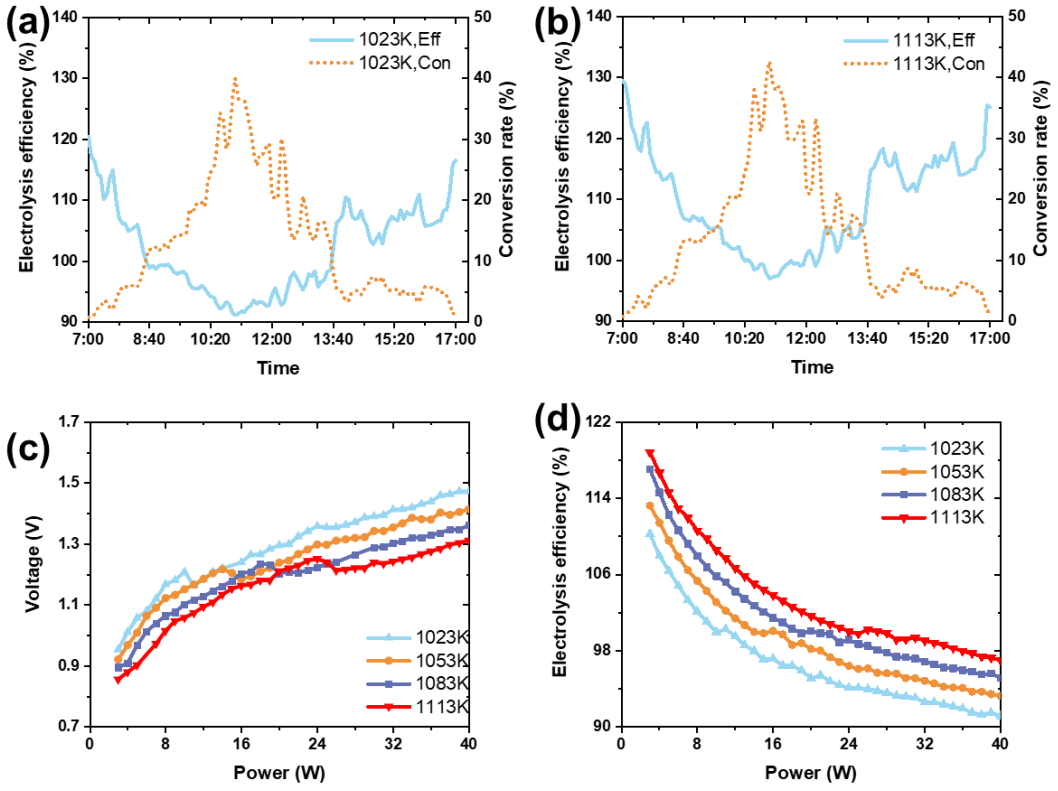

Fig. 8. Maximum gas flow rate while keeping the ratio of H_2:CO > 2:1 and electrolysis efficiency>90%. (a) the electrolysis efficiency and conversion rate at 1023 K - time relationship, (b) the electrolysis efficiency and conversion rate at 1113 K - time relationship, (c) the operating voltage changing with power at different temperatures, (d) the electrolysis efficiency changing with power at different temperatures.

4. Conclusion

In summary, we have developed a hybrid model to quickly simulate the operating parameters of SOECs when it works with a fluctuating renewable power supply, aiming at a safe and cost-effective operation by performing different optimizing strategies. We find the operating voltage is positively correlated with the input power at all temperatures and a higher inlet gas temperature contributes to a lower operating voltage in all the optimization strategies. Thermal neutral condition (TNC) can be achieved at different temperatures, where 1023 K, 1053 K, 1083 K and 1113 K are corresponded to the TNC power range of 10-16 W, 14-23 W, 18-29 W and 22-37 W, respectively. In the single object optimization strategy, the lowest maximum electrolysis efficiency is 94% at 1023K and 99% at 1113K, and highest maximum conversion rate can reach 100% at 11:00 with the highest power supply. But in multiple optimization objectives, target parameters such as the electrolysis efficiency and conversion rate can be slightly lower than that in the single object optimization. In the three-objective optimization, the highest conversion rate and the electrolysis efficiency only reach 40.1% and 91.2% at 1023K, respectively.

The combination of the experimental data, multi-physics simulation, artificial intelligence and optimization algorithm provides a novel method of model-based control systems for fast and accurate prediction and optimization of SOECs. This

method performs well in both single-objective optimization and multi-objective optimization and provides an advanced solution to the requirement for real-time optimization to complex control systems with proper modification.

5. Data and code availability

The database built based on validated MPS and the code for DNN are available at https://github.com/sw1122/SOEC-AI-Haoran-Xu.

Acknowledgement

The authors gratefully acknowledge the support from Zhejiang Provincial Key R&D Program (NO. 2022C01043) and the Zhejiang Provincial Natural Science Foundation (NO. LR20E060001). JX would like to acknowledge the financial support from EPSRC via grant numbers EP/V042432/1 and EP/V011863/1. M.NI also thanks the grants (Project Number: PolyU 152064/18E and N_PolyU552/20) from Research grant Council, University Grants Committee, Hong Kong SAR.

Supplementary material

Supplementary material related to this article can be found at attached file.

References

1. BP. Energy 2020 Outlook edition.
2. Torrell M, García-Rodríguez S, Morata A, Penelas G, Tarancón A. Co-electrolysis of steam and CO2 in full-ceramic symmetrical SOECs: a strategy for avoiding the use of hydrogen as a safe gas. FARADAY DISCUSS. 2015;182:241-255.
3. Chu S, Cui Y, Liu N. The path towards sustainable energy. NAT MATER. 2017;16:16-22.
4. Sherif SA, Barbir F, Veziroglu TN. Wind energy and the hydrogen economy - review of the technology. SOL ENERGY. 2005;78:647-660.
5. Dincer I. Technical, environmental and exergetic aspects of hydrogen energy

systems. INT J HYDROGEN ENERG. 2002;27:265-285.
6. Pan S, Chen Y, Fan L, Kim H, Gao X, Ling T, et al. CO2 mineralization and utilization by alkaline solid wastes for potential carbon reduction. Nature Sustainability. 2020;3:399-405.
7. Lin M, Han L, Singh MR, Xiang C. An Experimental- and Simulation-Based Evaluation of the CO2 Utilization Efficiency of Aqueous-Based Electrochemical CO2 Reduction Reactors with Ion-Selective Membranes. ACS Applied Energy Materials. 2019;2:5843-5850.
8. Takasu H, Maruyama Y, Kato Y. Development of Metal Supported SOEC for Carbon Recycling Iron Making System. ISIJ INT. 2020;60:2870-2875.
9. Wang Y, Liu T, Fang S, Xiao G, Wang H, Chen F. A novel clean and effective syngas production system based on partial oxidation of methane assisted solid oxide co-electrolysis process. J POWER SOURCES. 2015;277:261-267.
10. TING C, SHAORONG W. Water electrolysis using SOECs: A review. J CERAMICS. 2014;35:1-6.
11. Zhang X, O'Brien JE, O'Brien RC, Hartvigsen JJ, Tao G, Petigny N, et al. RECENT ADVANCES IN HIGH TEMPERATURE ELECTROLYSIS AT IDAHO NATIONAL LABORATORY: STACK TESTS. PROCEEDINGS OF THE ASME 10TH FUEL CELL SCIENCE, ENGINEERING, AND TECHNOLOGY CONFERENCE, 2012. 10th ASME Fuel Cell Science, Engineering and Technology Conference2012. p. 9-17.
12. Liang S, Altaf N, Huang L, Gao Y, Wang Q. Electrolytic cell design for electrochemical CO2 reduction. J CO2 UTIL. 2020;35:90-105.
13. Wang Y, Leung DYC, Xuan J, Wang H. A review on unitized regenerative fuel cell technologies, part B: Unitized regenerative alkaline fuel cell, solid oxide fuel cell, and microfluidic fuel cell. RENEW SUST ENERG REV. 2017;75:775-795.
14. Xu H, Chen B, Tan P, Zhang Y, He Q, Wu Z, et al. The thermal effects of all porous solid oxide fuel cells. J POWER SOURCES. 2019;440.
15. Mansilla C, Sigurvinsson J, Bontemps A, Marechal A, Werkoff F. Heat management for hydrogen production by high temperature steam electrolysis. ENERGY. 2007;32:423-430.
16. Dittrich L, Nohl M, Jaekel EE, Foit S, de Haart LGJB, Eichel R. High-Temperature Co-Electrolysis: A Versatile Method to Sustainably Produce Tailored Syngas Compositions. J ELECTROCHEM SOC. 2019;166:F971-F975.
17. Mesfun S, Sanchez DL, Leduc S, Wetterlund E, Lundgren J, Biberacher M, et al. Power-to-gas and power-to-liquid for managing renewable electricity intermittency in the Alpine Region. RENEW ENERG. 2017;107:361-372.
18. Cai Q, Adjiman CS, Brandon NP. Optimal control strategies for hydrogen production when coupling solid oxide electrolysers with intermittent renewable energies. J POWER SOURCES. 2014;268:212-224.
19. Xu H, Ma J, Tan P, Wu Z, Zhang Y, Ni M, et al. Enabling thermal-neutral electrolysis for CO2-to-fuel conversions with a hybrid deep learning strategy. ENERG CONVERS MANAGE. 2021;230.
20. Chen C, Xia Q, Feng S, Liu Q. A novel solar hydrogen production system integrating high temperature electrolysis with ammonia based thermochemical energy

storage. ENERG CONVERS MANAGE. 2021;237:114143.
21. Tebibel H. Methodology for multi-objective optimization of wind turbine/battery/electrolyzer system for decentralized clean hydrogen production using an adapted power management strategy for low wind speed conditions. ENERG CONVERS MANAGE. 2021;238:114125.
22. Wang Y, Banerjee A, Deutschmann O. Dynamic behavior and control strategy study of CO2/H2O co-electrolysis in solid oxide electrolysis cells. J POWER SOURCES. 2019;412:255-264.
23. Roh K, Chung W, Lee H, Park S, Lee JH. Impacts of deploying co-electrolysis of CO2 and H2O in the power generation sector: A case study for South Korea. Energy Reports. 2020;6:761-770.
24. Botta G, Romeo M, Fernandes A, Trabucchi S, Aravind PV. Dynamic modeling of reversible solid oxide cell stack and control strategy development. ENERG CONVERS MANAGE. 2019;185:636-653.
25. Han J, Wang X, Yan L, Dahlak A. Modelling the performance of an SOEC by optimization of neural network with MPSO algorithm. INT J HYDROGEN ENERG. 2019;44:27947-27957.
26. Cai Q, Adjiman CS, Brandon NP. Optimal control strategies for hydrogen production when coupling solid oxide electrolysers with intermittent renewable energies. J POWER SOURCES. 2014;268:212-224.
27. Andersson M, Yuan J, Sunden B. SOFC modeling considering electrochemical reactions at the active three phase boundaries. INT J HEAT MASS TRAN. 2012;55:773-788.
28. Guo M, Ru X, Lin Z, Xiao G, Wang J. Optimization Design of Rib Width and Performance Analysis of Solid Oxide Electrolysis Cell. ENERGIES. 2020;13.
29. Dumortier M, Sanchez J, Keddam M, Lacroix O. Theoretical considerations on the modelling of transport in a three-phase electrode and application to a proton conducting solid oxide electrolysis cell. INT J HYDROGEN ENERG. 2012;37:11579-11594.
30. Jin X, Xue X. Mathematical modeling analysis of regenerative solid oxide fuel cells in switching mode conditions. J POWER SOURCES. 2010;195:6652-6658.
31. Lin L, Chen S, Quan J, Liao S, Luo Y, Chen C, et al. Geometric synergy of Steam/Carbon dioxide Co-electrolysis and methanation in a tubular solid oxide Electrolysis cell for direct Power-to-Methane. ENERG CONVERS MANAGE. 2020;208.
32. Lin Q, Nadarajah S, Soheili N, Yang T. A Data Efficient and Feasible Level Set Method for Stochastic Convex Optimization with Expectation Constraints. J MACH LEARN RES. 2020;21.
33. Zamaniyan A, Joda F, Behroozsarand A, Ebrahimi H. Application of artificial neural networks (ANN) for modeling of industrial hydrogen plant. INT J HYDROGEN ENERG. 2013;38:6289-6297.
34. Zahadat P, Milewski J. Modeling electrical behavior of solid oxide electrolyzer cells by using artificial neural network. INT J HYDROGEN ENERG. 2015;40:7246-7251.
35. Zhang C, Liu Q, Wu Q, Zheng Y, Zhou J, Tu Z, et al. Modelling of solid oxide

electrolyser cell using extreme learning machine. ELECTROCHIM ACTA. 2017;251:137-144.
36. Cai M. Application Research of Artificial Intelligence in Electrical Automation Control. In Liu L, Xiao J, Zhou Y, "editors'. 2ND INTERNATIONAL CONFERENCE ON GREEN ENERGY AND SUSTAINABLE DEVELOPMENT (GESD 2019). 2nd International Conference on Green Energy and Sustainable Development (GESD)2019. p.
37. Recent advances and applications of machine learning in solidstate materials science. NPJ COMPUT MATER. 2021;5:1-36.
38. Tabor DP, Roch LM, Saikin SK, Kreisbeck C, Sheberla D, Montoya JH, et al. Accelerating the discovery of materials for clean energy in the era of smart automation. NAT REV MATER. 2018;3:5-20.
39. Poznyak A, Chairez I, Poznyak T. A survey on artificial neural networks application for identification and control in environmental engineering: Biological and chemical systems with uncertain models. ANNU REV CONTROL. 2019;48:250-272.
40. Hwangbo S, Nam K, Heo S, Yoo C. Hydrogen-based self-sustaining integrated renewable electricity network (HySIREN) using a supply-demand forecasting model and deep-learning algorithms. ENERG CONVERS MANAGE. 2019;185:353-367.
41. Xu H, Ma J, Tan P, Chen B, Wu Z, Zhang Y, et al. Towards online optimisation of solid oxide fuel cell performance: Combining deep learning with multi-physics simulation. Energy and AI. 2020;1:100003.
42. Hirth L. The market value of variable renewables. ENERG ECON. 2013;38:218-236.
43. Impacts of Variability and Uncertainty in Solar Photovoltaic Generation at Multiple Timescales.
44. Li W, Wang H, Shi Y, Cai N. Performance and methane production characteristics of H2O-CO2 co-electrolysis in solid oxide electrolysis cells. INT J HYDROGEN ENERG. 2013;38:11104-11109.
45. Xu H, Chen B, Irvine J, Ni M. Modeling of CH4-assisted SOEC for H2O/CO2 co-electrolysis. INT J HYDROGEN ENERG. 2016;41:21839-21849.
46. Xu H, Chen B, Tan P, Cai W, He W, Farrusseng D, et al. Modeling of all porous solid oxide fuel cells. APPL ENERG. 2018;219:105-113.